Physics Faculty Publications

Physics

4-1-1994

Ordering and fluctuations in the ground state of the one-dimensional and two-dimensional S = 1/2 XXZ antiferromagnets: A study of dynamical properties based on the recursion method

V. S. Viswanath
University of Rhode Island

Shu Zhang
University of Rhode Island

Joachim Stolze
University of Rhode Island

Gerhard Müller
University of Rhode Island, gmuller@uri.edu

Follow this and additional works at: https://digitalcommons.uri.edu/phys_facpubs

Ordering and fluctuations in the ground state of the one-dimensional and two-dimensional S = 1/2 XXZ antiferromagnets: A study of dynamical properties based on the recursion method

Publisher Statement

Terms of Use

Ordering and fluctuations in the ground state of the one-dimensional and two-dimensional $S = \frac{1}{2}$ XXZ antiferromagnets: A study of dynamical properties based on the recursion method

V.S. Viswanath, Shu Zhang, Joachim Stolze,* and Gerhard Müller

Department of Physics, The University of Rhode Island, Kingston, Rhode Island 02881-0817

The recursion method is applied to the $T = 0$ dynamics of the $S = \frac{1}{2}$ XXZ model on a linear chain and a square lattice. By means of new calculational techniques for the analysis of the continued-fraction coefficients pertaining to specific dynamical quantities, we obtain reliable information on the type of ordering in the ground state, on the size of gaps in the dynamically relevant excitation spectrum, on the bandwidths of dominant structures in spectral densities, on the exponents of infrared singularities, and on the detailed shape of spectral-weight distributions. We investigate some characteristic properties of the dynamic structure factors $S_{\mu\mu}(\mathbf{q}, \omega)$ and the spin autocorrelation functions $S^{\mu\mu}(\omega) = N^{-1} \sum_{\mathbf{q}} S_{\mu\mu}(\mathbf{q}, \omega)$, specifically their dependence on the uniaxial anisotropy, i.e., on the parameter which controls the type of ordering and the amount of quantum fluctuations in the ground state. We find, for example, that the different degrees of ordering in the planar regime of the one-dimensional and two-dimensional systems (criticality versus antiferromagnetic long-range order) have characteristic signatures in the dynamical properties which are conspicuously displayed in our results.

I. INTRODUCTION

The $S = 1/2$ XXZ model with bilinear antiferromagnetic coupling between nearest-neighbor spins on some lattice is specified by the Hamiltonian

$$H = \sum_{\langle i,j \rangle} \{ J(S_i^x S_j^x + S_i^y S_j^y) + J_z S_i^z S_j^z \} \tag{1.1}$$

for $J_z, J \geq 0$. It is an important model for magnetic insulators and plays a significant role as a limiting case of models used to describe systems of strongly correlated electrons (e.g., Hubbard model, t-J model).

For a given lattice, the degree of ordering in the ground state and the nature of the spectrum of low-lying excitations depend strongly on the type of exchange anisotropy (planar or uniaxial), which is controlled by the continuous parameter J_z/J. Schematic representations of the $T = 0$ phase diagrams (order parameter and spectral gaps) for the linear chain and the square lattice—the two cases we are concerned with in this study—are shown in Fig. 1.

For the one-dimensional (1D) system that sketch is based on rigorous results. The system is known to undergo a $T = 0$ phase transition between extended criticality at $J_z/J \leq 1$ (planar regime) and a state with antiferromagnetic long-range order at $J_z/J > 1$ (uniaxial regime). The ground-state energy and the excitation spectrum including the spectral gap have been determined via the Bethe ansatz.[1] The exact expression for the staggered magnetization $\bar{M}_z$ was a by-product of Baxter's work on 2D six-vertex models.[2] The critical exponents which characterize the susceptibilities and integrated intensities at $q = \pi$ and the infrared singularities in various dynamical quantities throughout the planar

regime depend continuously on the anisotropy parameter J_z/J. That functional dependence was investigated and rigorously established along several different paths.[3]

Despite a wealth of exact results for *static* $T = 0$ properties, the determination of *dynamical* correlation functions has remained an elusive goal except for the case $J_z/J = 0$, which can be interpreted as a model of free lattice fermions. But even for that case the evaluation of some dynamical quantities is exceedingly

(a) linear chain
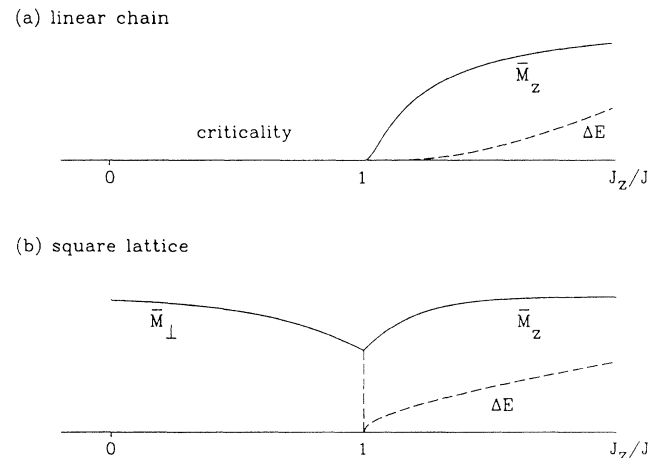

(b) square lattice

FIG. 1. Phase diagrams of the 1D and 2D $S = 1/2$ XXZ antiferromagnets in a schematic representation: J_z/J dependence of the staggered magnetization $\bar{M}_z$ or $\bar{M}_\perp$ (solid lines) and of the spectral gap ΔE between the ground state and the lowest branch of excitations at $q = \pi$ or $\mathbf{q} = (\pi, \pi)$, respectively (dashed lines).

complicated because of the subtle relationship between fermion operators and spin operators.[4] The few existing exact expressions for frequency-dependent spin correlation functions[5,6] are an ideal testing ground for the various calculational techniques that are being used to tackle the more formidable tasks of investigating the dynamics of models with few or no guideposts of rigorous knowledge.

Exact results for the 2D XXZ model have essentially been limited to existence proofs for long-range order in the ground state. At this time, published proofs[7-10] cover the entire parameter range excluding the vicinity ($0.22 \leq J_z/J \leq 1.47$) of the isotropic case, but the consensus is that the XXZ model on the square lattice is antiferromagnetically ordered for all values $J_z/J \geq 0$.[11-14] Consequently there must be a transition, logically at the symmetry point $J_z/J = 1$, involving a 90° rotation of the order parameter (from $\bar{M}_z \neq 0$ to $\bar{M}_\perp \neq 0$). In order for that to happen, the spectral gap ΔE must go to zero as J_z/J approaches unity from above. At $J_z/J \leq 1$, the spectral gap stays zero because the order parameter $\bar{M}_\perp$ now breaks a continuous symmetry of H.

Since the staggered magnetization does not commute with the Hamiltonian, its magnitude is reduced from the saturation value, and the ground state contains a certain amount of correlated quantum fluctuations except in the Ising limit $J_z/J \to \infty$. As the anisotropy parameter decreases toward $J_z/J = 1$, the quantum fluctuations gain strength and cause an increasing amount of spin reduction. In the 1D system, they make the long-range order disappear completely at the symmetry point. Moreover, the planar anisotropy does not weaken them sufficiently to allow an in-plane staggered magnetization to establish itself for $J_z/J < 1$. In the 2D system, by contrast, the quantum fluctuations lead to only a partial spin reduction anywhere on the J_z/J axis. The magnitude of the order parameter is expected to have a minimum for isotropic exchange coupling.[15,16]

It is interesting to compare the impact of zero-point *quantum fluctuations* on the antiferromagnetic ordering with the impact of *thermal fluctuations* at small nonzero temperature. In the planar regime ($J_z/J \leq 1$), 2D long-range order is stable against the former ($T = 0$) but, according to the Mermin-Wagner theorem,[17] not against the latter ($T > 0$), whereas 1D long-range order is nonexistent even at $T = 0$. In the uniaxial regime ($J_z/J \geq 1$), the 1D and 2D staggered magnetizations both survive the zero-point motion, but only the 2D order parameter can withstand some amount of thermal fluctuations.

The different types of zero-temperature phase transition that take place at $J_z/J = 1$ in the 1D and the 2D $S = 1/2$ antiferromagnets and the different degrees of ordering at $J_z/J \leq 1$ are reflected in the dynamical properties by unmistakable signatures. The goal of this study is to determine and elucidate these signatures by means of the recursion method.

II. RECURSION METHOD

The recursion method[18,19] as applied to problems in quantum many-body dynamics[20-22] is a general calcu-

lational technique with virtually no intrinsic restrictions. For a given model system, the recursion method provides (in the context of this study) an algorithm for the computation of the sequence of continued-fraction coefficients pertaining to any zero-temperature dynamic quantity of interest. The input into the recursion algorithm consists of (i) the Hamiltonian operator and its ground-state wave function for a system of finite size, $H|\phi_0\rangle = E_0|\phi_0\rangle$, and (ii) the operator A representing the dynamical variable of interest. The finite-size ground-state wave function can be determined by standard algorithms based on the Lanczös method[21,23] or (for enhanced convergence) the conjugate-gradient method.[24,25]

A. Orthogonal expansion of wave functions

The Hamiltonian representation of the recursion method for the determination of the *correlation function*

$$\tilde{S}(t) = \langle\phi_0|A^\dagger(t)A|\phi_0\rangle = \langle\phi_0|A^\dagger A(-t)|\phi_0\rangle \quad (2.1)$$

is based on an orthogonal expansion of the wave function,[21]

$$|\psi(t)\rangle \equiv A(-t)|\phi_0\rangle = \sum_{k=0}^{\infty} D_k(t)|f_k\rangle. \quad (2.2)$$

The orthogonal basis $\{|f_k\rangle\}$ is determined recursively from the initial state $|f_0\rangle = A|\phi_0\rangle$ with the Hamiltonian $\bar{H} \equiv H - E_0$ as the generator of new directions:

$$|f_{k+1}\rangle = \bar{H}|f_k\rangle - a_k|f_k\rangle - b_k^2|f_{k-1}\rangle, \quad k = 0, 1, 2, \ldots,$$
$$(2.3a)$$

$$a_k = \frac{\langle f_k|\bar{H}|f_k\rangle}{\langle f_k|f_k\rangle}, \quad k = 0, 1, 2, \ldots, \quad (2.3b)$$

$$b_k^2 = \frac{\langle f_k|f_k\rangle}{\langle f_{k-1}|f_{k-1}\rangle}, \quad k = 1, 2, \ldots, \quad (2.3c)$$

with $|f_{-1}\rangle \equiv 0$. The expansion (2.2) is then inserted into the Schrödinger equation, $i(\partial/\partial t)|\psi(t)\rangle = \bar{H}|\psi(t)\rangle$ This results in a set of coupled linear differential equations for the functions $D_k(t)$, which, upon Laplace transform,

$$d_k(\zeta) \equiv \int_0^\infty dt e^{i\zeta t} D_k(t), \quad (2.4)$$

can be solved for $d_0(\zeta)$ in the continued-fraction representation,

$$d_0(\zeta) = \cfrac{i}{\zeta - a_0 - \cfrac{b_1^2}{\zeta - a_1 - \cfrac{b_2^2}{\zeta - a_2 - \ldots}}}, \quad (2.5)$$

and from which the *structure function*

$$S(\omega) \equiv \int_{-\infty}^{+\infty} dt\, e^{i\omega t}\tilde{S}(t) \tag{2.6}$$

is then directly recovered via the relation

$$S(\omega) = 2\langle\phi_0|A^\dagger A|\phi_0\rangle \lim_{\varepsilon\to 0}\Re[d_0(\omega + i\varepsilon)]. \tag{2.7}$$

B. Orthogonal expansion of dynamical variables

The Liouvillian representation of the recursion method for the determination of the *fluctuation function*,

$$\tilde{\Phi}(t) = \tfrac{1}{2}[\tilde{S}(t) + \tilde{S}(-t)], \tag{2.8}$$

provides an alternative algorithm based on an orthogonal expansion of the dynamical variable,[20]

$$A(t) = \sum_{k=0}^{\infty} C_k(t)f_k. \tag{2.9}$$

The orthogonal basis $\{f_k\}$ is obtained recursively from $f_0 = A$ with the Liouvillian $L = [H, \ ]$ as the generator of new directions:

$$f_{k+1} = iLf_k + \Delta_k f_{k-1}\ , \quad k = 0, 1, 2, \ldots, \tag{2.10a}$$

$$\Delta_0 = 0\ , \quad \Delta_k = \frac{(f_k, f_k)}{(f_{k-1}, f_{k-1})}\ , \quad k = 1, 2, \ldots, \tag{2.10b}$$

with the inner product

$$(f_k, f_l) \equiv \tfrac{1}{2}\langle\phi_0|f_k^\dagger f_l + f_l f_k^\dagger|\phi_0\rangle. \tag{2.11}$$

The expansion (2.9), inserted into the Heisenberg equation, $dA/dt = iLA$, yields a set of coupled linear differential equations for the functions $C_k(t)$, which can be solved, after Laplace transform,

$$c_k(z) \equiv \int_0^\infty dt\, e^{-zt}C_k(t), \tag{2.12}$$

for the *relaxation function* $c_0(z)$ in the continued-fraction representation,

$$c_0(z) = \cfrac{1}{z + \cfrac{\Delta_1}{z + \cfrac{\Delta_2}{z + \ldots}}}. \tag{2.13}$$

The (normalized) *spectral density*, which is the Fourier transform of the normalized fluctuation function,

$$\Phi_0(\omega) \equiv \int_{-\infty}^{+\infty} dt\, e^{i\omega t}C_0(t)\ , \quad C_0(t) = \frac{\tilde{\Phi}(t)}{\tilde{\Phi}(0)}, \tag{2.14}$$

can be recovered directly from the relaxation function:

$$\Phi_0(\omega) = \lim_{\varepsilon\to 0} 2\Re[c_0(\varepsilon - i\omega)]. \tag{2.15}$$

C. Nearly size-independent Δ_k sequences

The results obtained from the two representations of the recursion method are equivalent in principle. The fluctuation function (2.8) is equal to the (symmetric) real part of the correlation function (2.1) and determines, by virtue of the Kramers-Kronig relations, also the (antisymmetric) imaginary part of (2.1). At zero temperature, this translates into the following relation between the (one-sided) structure function (2.6) and the (symmetric) spectral density (2.14):

$$S(\omega) = 2\langle\phi_0|A^\dagger A|\phi_0\rangle\Phi_0(\omega)\Theta(\omega) \quad (T = 0). \tag{2.16}$$

The relation between the continued fractions (2.5) and (2.13) can be expressed in terms of transformation formulas between the respective coefficients (see Appendix A for details).

Employing the Hamiltonian or the Liouvillian representation of the recursion method in a given application is a matter of computational convenience, but for the interpretation and further analysis of the information thus obtained, processing the single Δ_k sequence determined directly (Sec. II B) or indirectly (Sec. II A and Appendix A) offers important advantages over processing the double sequence $\{a_k, b_k^2\}$.

Whereas many properties of the ground state are strongly dependent on the system size N (here the number of spins), there exists for each dynamic quantity a number of coefficients Δ_k that are at most very weakly size dependent.[26] For the continued-fraction analysis proposed here we discard all but the nearly size-independent Δ_k's. The relatively small number of available nearly N-independent Δ_k's limits the precision of the predictions that can be made. Our experience shows that these limitations are benign compared to the problems that arise when strongly N-dependent Δ_k's are included in the analysis. In all applications discussed here, the nearly size-independent Δ_k's exhibit some more or less clearly recognizable pattern that translates into a specific property of the associated spectral density (2.15). We may call this pattern the *implicit* information extractable from the sequence $\Delta_1, \ldots, \Delta_K$ in addition to the *explicit* information contained in these K values.

D. Model spectral densities

A common occurrence in quantum many-body dynamics are Δ_k sequences that grow linearly with k on average. This property translates into spectral densities with unbounded support and a Gaussian decay law for the spectral weight at high frequencies.[27,28] The patterns which are typical for the applications discussed in this study can all be generated from one of two model spectral densities.

The first model spectral density is of the form

$$\bar{\Phi}_0(\omega) = \frac{2\pi}{\omega_0\Gamma(\alpha/2 + 1/2)}\left|\frac{\omega}{\omega_0}\right|^\alpha \exp(-\omega^2/\omega_0^2). \tag{2.17}$$

The $\bar{\Delta}_k$ sequence inferred from its frequency moments is

known in closed form:[29]

$$\bar{\Delta}_{2k-1} = \tfrac{1}{2}\omega_0^2(2k-1+\alpha) \ , \quad \bar{\Delta}_{2k} = \tfrac{1}{2}\omega_0^2(2k). \quad (2.18)$$

The slope of the line $\bar{\Delta}_{2k}$ determines the characteristic frequency ω_0, and the vertical displacement of the $\bar{\Delta}_{2k-1}$ from that line determines the exponent α of the infrared singularity. The model spectral density (2.17) is displayed in Fig. 2 for a positive and a negative value of α along with the corresponding $\bar{\Delta}_k$ sequences in the insets. These characteristic patterns (henceforth called 1A for $\alpha < 0$ and 1B for $\alpha > 0$) are typical in applications to dynamical quantities associated with critical fluctuations. In fact, type-1 Δ_k sequences are useful indicators for the identification and location of critical points in $T = 0$ phase diagrams of quantum many-body systems. They can also be used to estimate the values of critical exponents (Sec. III C).

The second model spectral density relevant in the context of this study reads

$$\bar{\Phi}_0(\omega) = 2\pi A\delta(\omega) + \frac{2\sqrt{\pi}}{\omega_0}(1-A)\Theta(|\omega|-\Omega)e^{-\frac{(|\omega|-\Omega)^2}{\omega_0^2}} .$$

$$(2.19)$$

It has unbounded support and a gap of width 2Ω centered at $\omega = 0$. An isolated spectral line with intensity $A \geq 0$ is located at the center of the gap. For $A = 0$ and $\Omega = 0$, expression (2.19) reduces to a pure Gaussian, whose $\bar{\Delta}_k$ sequence grows linearly with k, $\bar{\Delta}_k = \omega_0^2k/2$. The effect of the gap is to split the $\bar{\Delta}_k$ sequence into two subsequences $\bar{\Delta}_{2k}$ and $\bar{\Delta}_{2k-1}$ that still grow (roughly) linearly, but with different slopes. In the absence of a central peak, the $\bar{\Delta}_{2k-1}$ grow more steeply than the $\bar{\Delta}_{2k}$ (type 2A). If the $\bar{\Delta}_{2k}$ grow more steeply (at least for large k), this is a sure indicator that a central peak is present (type 2B). We do not know the $\bar{\Delta}_k$ sequence of the model spectral density (2.19) in closed form, but it can be generated numerically from the exact frequency
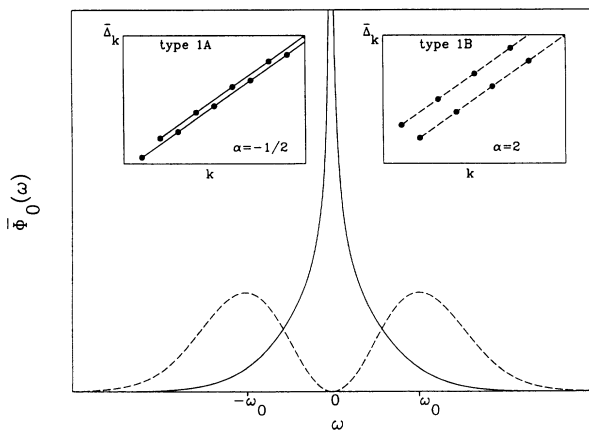

FIG. 2. Model spectral density (2.17) with unbounded support and power-law behavior at low frequencies for the two cases $\alpha = -1/2$ (solid lines) and $\alpha = 2$ (dashed lines). The $\bar{\Delta}_k$ sequences (2.18) for the two cases are displayed in the insets.
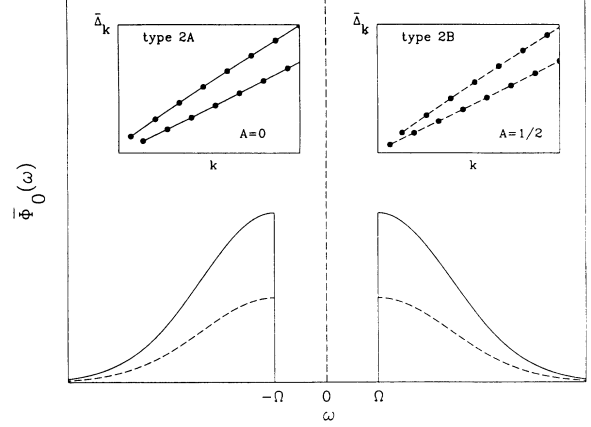

FIG. 3. Model spectral density (2.19) with unbounded support and a gap for the two cases $A = 0$, $\omega_0 = 2\Omega$ (solid lines) and $A = 1/2$, $\omega_0 = 2\Omega$ (dashed lines). The $\bar{\Delta}_k$ sequences for the two cases are displayed in the insets.

moments as described in Appendix A. Two prototypical cases are displayed in Fig. 3.[30]

In applications of the recursion method, these type-2 patterns play an important role in identifying the presence of long-range order in the ground state[31] and in identifying the dynamical variable associated with that long-range order. Type-2 patterns also occur in the analysis of dispersion curves of low-lying excitations that dominate certain spectral densities.

E. Reconstruction of spectral densities

The calculational scheme proposed here has been designed to incorporate the explicit and the implicit information contained in a sequence $\Delta_1, \ldots, \Delta_K$ of nearly size-independent continued-fraction coefficients to the fullest extent possible into the reconstructed spectral density. The method is best described in terms of three different relaxation functions, each expanded into a continued fraction down to level K.

The *exact relaxation function*

$$c_0(z) = \cfrac{1}{z + \cfrac{\Delta_1}{z + \cfrac{\ddots}{\ddots + \cfrac{\Delta_{K-1}}{z + \Delta_K\Gamma_K(z)}}}} \quad (2.20)$$

is the one we wish to determine, here expressed in terms of *explicitly* known coefficients $\Delta_1, \ldots, \Delta_K$ obtained from the recursion method, and an unknown termination function $\Gamma_K(z)$.

The *model relaxation function* $\bar{c}_0(z)$ expressed in terms of K model coefficients $\bar{\Delta}_1, \ldots, \bar{\Delta}_K$ and a model termination function $\bar{\Gamma}_K(z)$ is determined via

$$\bar{c}_0(z) = \frac{1}{2\pi i}\int_{-\infty}^{+\infty} d\omega \frac{\bar{\Phi}_0(\omega)}{\omega - iz} \quad (2.21)$$

from one of the two model spectral densities (2.17) or (2.19) with its parameters determined by fitting the model $\bar{\Delta}_k$ sequence of the correct type to the known sequence of nearly size-independent Δ_k's. The function $\bar{c}_0(z)$ thus incorporates the *implicit* information contained in the latter.

The *reconstructed relaxation function* $\bar{c}_0(z)$, finally, is obtained by substituting the known, matching termination function $\bar{\Gamma}_K(z)$ for the unknown function $\Gamma_K(z)$ in (2.20). This function thus combines the *explicit* information from $c_0(z)$ and the *implicit* information from $\bar{c}_0(z)$ consistently and comprehensively. Furthermore it screens out finite-size effects to a considerable extent. Remarks on practical aspects of the reconstruction procedure are found in Appendix B.

III. 1D $S = 1/2$ XXZ MODEL
IN THE PLANAR REGIME

The 1D case of Hamiltonian (1.1) has a critical ground state throughout the planar regime $0 \leq J_z/J \leq 1$, as noted previously (see Fig. 1). The two-spin equal-time correlation functions are known to decay algebraically at large distances,

$$\langle S_l^\mu S_{l+n}^\mu \rangle \sim (-1)^n n^{-\eta_\mu}. \tag{3.1}$$

The critical exponents $\eta_x = \eta_y$ and η_z depend continuously on J_z/J:[3]

$$\eta_z = 1/\theta, \quad \eta_x = \theta, \tag{3.2a}$$

$$\theta = 1 - \frac{1}{\pi}\arccos(J_z/J). \tag{3.2b}$$

The spectrum of low-lying excitations most relevant for the $T = 0$ dynamical quantities discussed here has the form of a two-parameter continuum consisting of two partly overlapping sheets with a common lower boundary,

$$\varepsilon_L(q) = \frac{\pi J \sin \vartheta}{2\vartheta}|\sin q| \ , \quad \cos \vartheta = J_z/J, \tag{3.3a}$$

and two separate upper boundaries,[32]

$$\varepsilon_U(q) = \frac{\pi J \sin \vartheta}{\vartheta}|\sin \frac{q}{2}| = \bar{\varepsilon}_U(\pi - q). \tag{3.3b}$$

The critical nature of the ground state manifests itself in characteristic (power-law) infrared singularities (with J_z/J-dependent exponents) in all those dynamical quantities that are susceptible to the critical fluctuations, specifically the dynamic structure factor $S_{xx}(q, \omega)$ at $q = \pi$ and the frequency-dependent spin autocorrelation function $S^{xx}(\omega)$.

A. Dynamic structure factor $S_{xx}(q, \omega)$

For the reconstruction of the dynamic structure factor $S_{xx}(q, \omega)$ we have consistently used $K = 6$ nearly size-independent Δ_k's extracted by means of the recursion

method from the ground-state wave function of a system with $N = 16$ spins. The results of the reconstruction are plotted in Figs. 4(a)–(c) for three values of J_z/J. The Δ_k's are of type 2A at $0 < q < \pi$, which indicates a spectral gap. Therefore we use the model spectral density (2.19) with $A = 0$ to reconstruct $S_{xx}(q, \omega)$ as outlined in Sec. II E. At $q = \pi$, the Δ_k sequence is of type 1A, which signals zero gap and a divergent singularity at $\omega = 0$. Here we employ the (Gaussian) model spectral density (B3).[33] In order to recover the dynamic structure factor $S_{xx}(q, \omega)$ at $\omega > 0$, i.e., the structure function (2.6) from the reconstructed spectral density (2.15), we have to multiply the latter by twice the integrated intensity $\langle S_q^x S_{-q}^x \rangle$ ($= \langle f_0|f_0\rangle$ in the recursion algorithm).

Let us first discuss the results for the case $J_z/J = 1$, which are depicted in Fig. 4(a). We observe that almost all the spectral weight is distributed between the continuum boundaries $\varepsilon_L(q)$ and $\varepsilon_U(q)$ [indicated by circles in the (q, ω) plane]. The reconstructed $S_{xx}(q, \omega)$ is strongly peaked at $\omega \simeq \varepsilon_L(q)$, and there exists a conspicuous tail of spectral weight tapering off at $\omega \simeq \varepsilon_U(q)$. The q-dependent gap of size $\varepsilon_L(q)$ is very reliably reproduced for all q values. We should like to emphasize that for the results shown in Fig. 4(a) the value of the gap parameter Ω in the model spectral density (2.19) was inferred from the nearly size-independent Δ_k's and not externally set equal to $\varepsilon_L(q)$.

From the stability of these results under variations of the numerical analysis, we conclude that they are largely free of artificial structures. The only exceptions are perhaps the weak secondary maxima at $q = 5\pi/8$ and $6\pi/8$, mainly because we do not have an interpretation for their presence. Since the reconstruction is based exclusively on the nearly size-independent Δ_k's, the curves do not reflect the unwanted effects of the discrete finite-size spectrum.[34]

The reconstructed $S_{xx}(\pi, \omega)$ suggests the presence of a strong infrared divergence. This is indeed rigorously known to be the case and attributable to the critical fluctuations. Thermal fluctuations are expected to remove the infrared divergence in $S_{xx}(\pi, \omega)$, but it is doubtful that the peak should move away from $\omega = 0$ as suggested by the quantum Monte Carlo results of Ref. 35.

The reconstructed dynamic structure factors $S_{xx}(q, \omega)$ for $J_z/J = 0.5$ and $J_z/J = 0$ are shown in Figs. 4(b) and 4(c), respectively. In order to correct for some not so accurate gap estimates in these two cases, we have set the parameter Ω in the model spectral density (2.19) equal to $\varepsilon_L(q)$, the known exact threshold of the excitation spectrum. This accounts for the sharper edge in the spectral-weight distributions at $\omega = \varepsilon_L(q)$ in Figs. 4(b), (c) as compared to (a).[36]

What is the effect of planar anisotropy on the dynamic structure factor $S_{xx}(q, \omega)$ as reflected in the results of Fig. 4? For $J_z/J < 1$, a significant amount of spectral weight is transferred to the second sheet [with upper boundary $\bar{\varepsilon}_U(q)$] of the two-parameter continuum. This effect is best visible at small q. The integrated intensity $\langle S_q^x S_{-q}^x \rangle$ is nonzero for $q = 0$. There is no longer a conservation law which prohibits that from happening. The line shapes strongly suggest that the spectral-weight

distribution is divergent at the lower continuum boundary $\varepsilon_L(q)$ throughout the planar regime. This confirms the conclusions of an early finite-chain study of XXZ dynamics.[32] The mild enhancement of spectral weight at the continuum boundary $\bar{\varepsilon}_U(q)$, best visible in Fig. 4(c), is attributable to a divergent density of states at the upper edge of the two-parameter continuum.

Let us conclude with a remark on the dynamic structure factor $S_{zz}(q,\omega)$, which has been the object of more extensive studies based on a variety of approaches (complete numerical diagonalization of finite chains,[32,37,38] sum rules,[39,40] lattice fermions,[38,41,42] Fermi fields,[43] bosonization[44]). The results of those studies have led to a consistent picture, according to which the function $S_{zz}(q,\omega)$ has almost all of its spectral weight confined between the boundaries $\varepsilon_L(q)$ and $\varepsilon_U(q)$. In Refs. 32 and 40, an explicit expression for $S_{zz}(q,\omega)$ was proposed for the spectral-weight distribution within the range of the two-parameter continuum, which connects smoothly with the known exact result[5] for $J_z/J = 0$ and exhibits the right singularity at $q \simeq \pi$. That expression for $J_z/J = 1$ was recently found to provide a near perfect match with the data of an inelastic neutron scattering experiment by Nagler *et al.*[45] on the quasi-1D compound $KCuF_3$.

The free-fermion nature of the exactly solvable case $J_z/J = 0$ poses a problem for the reconstruction of the function $S_{zz}(q,\omega)$ in that the fermion interaction causes a crossover between different patterns in the Δ_k sequences. This has the consequence that none of the model spectral densities introduced in Sec. II D is applicable over much of the planar regime $(0.5 \lesssim J_z/J \lesssim 0.9)$. However, for sufficiently weak coupling $(J_z/J \lesssim 0.5)$, new oppor-
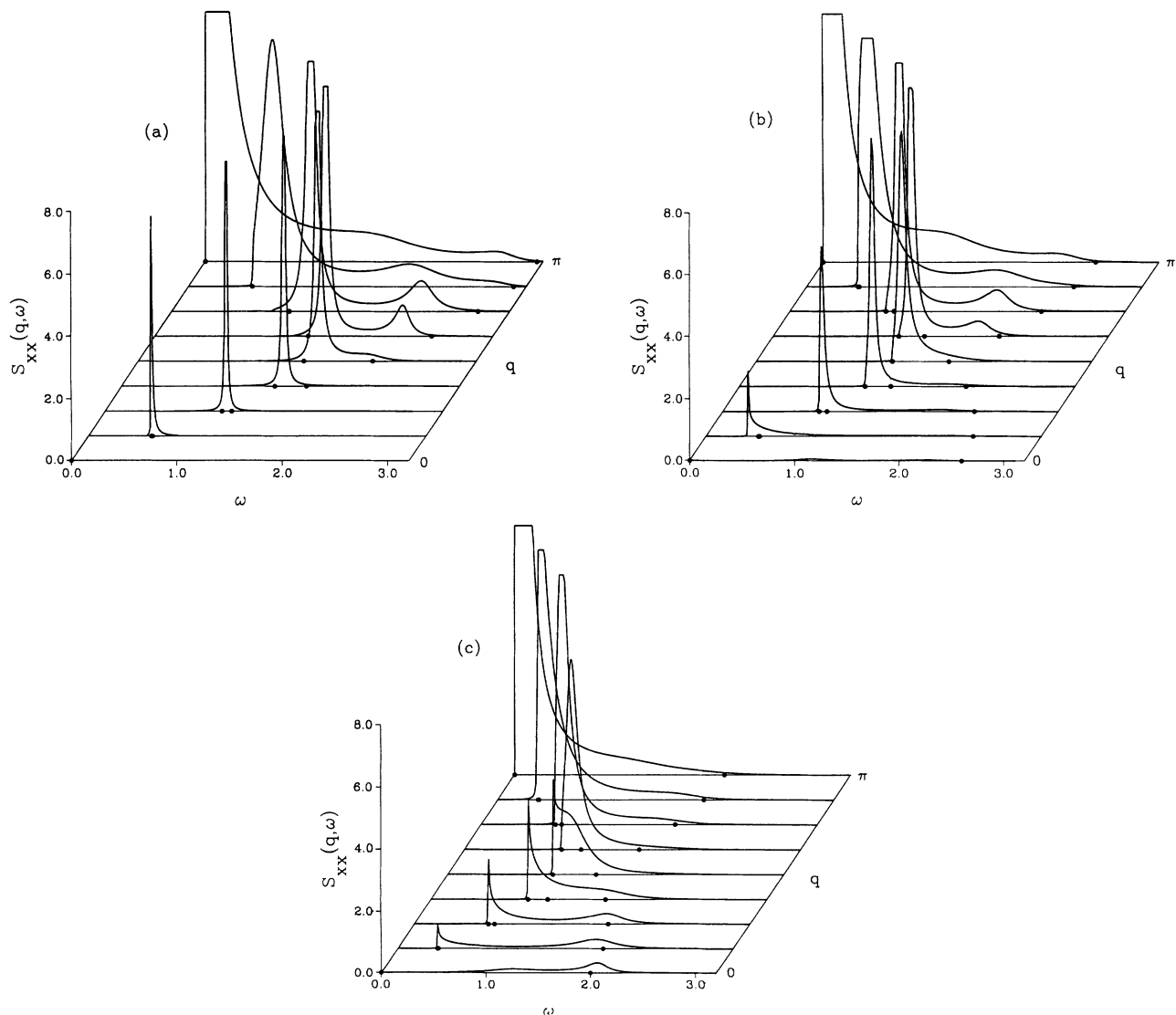

FIG. 4. Dynamic structure factor $S_{xx}(q,\omega)$ at $T = 0$ for fixed $q = n\pi/8, n = 0, 1, \ldots, 8$ of the 1D $S = 1/2$ XXZ antiferromagnet with $J = 1$ and (a) $J_z = 1$, (b) $J_z = 0.5$, and (c) $J_z = 0$. The results were derived from the reconstructed relaxation function $\tilde{c}_0(z)$ with six nearly size-independent continued-fraction coefficients Δ_k and a judiciously selected termination function as described in the text. The circles in the (q,ω) plane indicate the boundaries (3.3) of the two-parameter continuum of dominant excitations.

tunities present themselves for an alternative continued-fraction analysis with enhanced precision.[46]

B. Spin autocorrelation function $S^{xx}(\omega)$

The frequency-dependent spin autocorrelation function,

$$S^{xx}(\omega) \equiv \int_{-\infty}^{\infty} dt e^{i\omega t} \langle S_l^x(t) S_l^x \rangle = \int_{-\pi}^{+\pi} \frac{dq}{2\pi} S_{xx}(q, \omega),$$

$$(3.4)$$

subjected to its own continued-fraction analysis, provides further insight into the dynamics of the XXZ chain. Starting from the same finite-size ground-state wave function for a ring of $N = 18$ spins, we have determined $K = 7$ nearly size-independent Δ_k's for the operator $A = S_l^x$ in expression (2.1). Here we are dealing with type-1 Δ_k-sequences (no gap!). In an effort to be as unbiased as possible with respect to the spectral-weight distribution emerging from the reconstruction process, we have employed the Gaussian model spectral density (B3) with ω_0 determined by a one-parameter fit. The results of this reconstruction are depicted in Fig. 5. The six curves on the left pertain to the values 0, 0.1,...,0.5 of the exchange anisotropy J_z/J and the five curves on the right to the values 0.6,...,1.0.

The reconstructed $S^{xx}(\omega)$ evolves rather smoothly with varying J_z/J. None of the observed structures are artificially imposed by our choice of termination function, nor are they artifacts by nature. An exact result exists only at $J_z/J = 0$.[6] It was inferred by means of special methods which exploit the free-fermion nature of the ex-

citation spectrum. In a previous study,[22] we have used that exact result as a benchmark test for the recursion method and our continued-fraction analysis.

The enhancement of spectral weight at low frequencies signals the presence of an infrared divergence with variable strength. It is strongest at $J_z/J = 0$ and weakens monotonically with increasing J_z/J. The exact result for $J_z/J = 0$ has a square-root infrared divergence. The J_z/J dependence of that singularity will be further analyzed in Sec. III C.

Now consider the peak at $\omega/J \gtrsim 1$. Note that its position moves monotonically to higher frequencies as J_z/J increases from 0 to 1. That peak echoes a divergent singularity of some kind at $\omega = \varepsilon_L(\pi/2)$. The peak position is, in fact, very close to that frequency throughout the parameter range, as indicated by the marks on the auxiliary axes. That singularity is a consequence of the singularity in $S_{xx}(q, \omega)$ along the spectral threshold $\varepsilon_L(q)$.

The variable strength of the peak at $\omega/J \gtrsim 1$ might indicate that the associated singularity is also characterized by a J_z/J-dependent exponent like the one at $\omega = 0$.[47] If that is so, then the results of Fig. 5 indicate that with J_z increasing from zero, the singularity gains strength at least initially (up to $J_z/J \simeq 0.5$). Since the singularity at $\omega = 0$ is rigorously known to lose strength with increasing J_z, that observation would imply that the divergence at $\omega = \varepsilon_L(q)$ in the dynamic structure factor $S_{xx}(q, \omega)$ is not characterized by one and the same exponent for different values of q.

For $J_z/J = 0$, the function $S^{xx}(\omega)$ is known to have a further detectable singularity—a square-root cusp at $\omega = 2J$. In the curves of Fig. 5 there is indeed a hint of structure at or near the upper continuum boundary $\varepsilon_U(\pi) = \bar{\varepsilon}_U(0)$. There is very little spectral weight beyond that frequency, which further underlines the importance of the two-parameter continuum bounded by the branches (3.3) for the $T = 0$ dynamics of the 1D $S = 1/2$ XXZ model.

Let us add a word here on the function $S^{zz}(\omega)$. For $J_z/J = 0$ it is exactly known[5] and expressible in terms of elliptic integrals.[6] Not much is known about its structure for $J_z/J > 0$ other than the exponent of its infrared singularity (to be discussed in Sec. III C). The continued-fraction analysis of this function is subject to the same type of complications and offers the same kind of alternatives as previously mentioned in the context of the function $S_{zz}(q, \omega)$.[46]
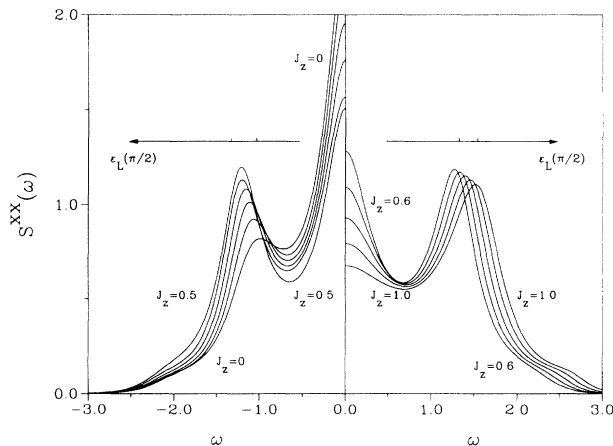

FIG. 5. Spin autocorrelation function $S^{xx}(\omega)$ at $T = 0$ of the 1D $S = 1/2$ XXZ antiferromagnet with $J = 1$ and $J_z = 0, 0.1, \ldots, 1.0$. The results are derived from the reconstructed relaxation function $\bar{c}_0(z)$ with seven nearly size-independent continued-fraction coefficients Δ_k and a judiciously selected termination function as described in the text. The tick marks on the auxiliary horizontal axes inside the figure indicate the range of values of $\varepsilon_L(\pi/2)$ for the J_z values selected on either side of the figure.

C. Infrared singularities in $S_{\mu\mu}(\pi, \omega)$ and $S^{\mu\mu}(\omega)$

The critical nature of the ground state of the 1D $S = 1/2$ XXZ model in the planar regime manifests itself not only in terms of algebraically decaying equal-time correlation functions $\langle S_l^\mu S_{l+n}^\mu \rangle$ or, equivalently, power-law singularities in the corresponding integrated intensities $\langle S_q^\mu S_{-q}^\mu \rangle$, but also in terms of power-law infrared singularities in specific structure functions such as $S_{\mu\mu}(\pi, \omega)$ and $S^{\mu\mu}(\omega)$. Both types of singularities describe different aspects of the same critical fluctuations and are characterized by interrelated sets of critical exponents. For the

model at hand, these exponents are continuous functions of J_z/J. The explicit results for the exponents η_x, η_z of the equal-time correlation functions have already been quoted in (3.2). For the structure functions we have

$$S^{\mu\mu}(\omega) \sim \omega^{\alpha_\mu}, \quad S_{\mu\mu}(\pi,\omega) \sim \omega^{\beta_\mu}, \qquad (3.5)$$

with

$$\alpha_z = \beta_z + 1 = \frac{1}{\theta} - 1, \quad \alpha_x = \beta_x + 1 = \theta - 1, \qquad (3.6)$$

and the parameter θ from (3.2b). The relation between the static exponents η_μ and the dynamic exponents α_μ, β_μ is established by the Lorentz invariance of the Fermi field theory which was shown to describe the long-distance and long-time properties of the XXZ chain:[43,44]

$$\langle S_l^\mu(t) S_{l+n}^\mu \rangle \sim (-1)^n [n^2 - c^2 t^2]^{-\frac{1}{2}\eta_\mu}. \qquad (3.7)$$

An exact determination of the exponents describing the critical ground state of a quantum many-body system is in general out of reach. Therefore, the availability of a general method by which the exponents of infrared singularities in spectral densities can be estimated with reasonable accuracy is an asset of considerable value. The recursion method is such a method. Here we use it to estimate the exponents α_μ, β_μ of the $S = 1/2$ XXZ chain in a test application that shows its strengths and limitations. A different general method, based on Luck's formula, was previously employed by Schulz and Ziman[48] with considerable success for the determination of the exponents η_x, η_z from finite-size data for the energies of the ground state and and two specific low-lying excitations. In our approach, by contrast, the infrared exponents are derived from the finite-size ground-state wave function.

The assumption is that the nearly size-independent sequence $\Delta_1, \ldots, \Delta_K$ to be analyzed exhibits a type-1 pattern. If that is the case, we determine the singularity exponent by using the model sequence (2.18) as follows: At first the slope parameter ω_0 is determined by a straight-line fit to $\Delta_1, \ldots, \Delta_K$.[49] For every possible pair of one Δ_{2k} and one Δ_{2k-1} the vertical displacement between lines (of slope $\omega_0^2/2$) going through the two data points is then determined. Finally, the average (over all pairs) of those displacements is used to determine the singularity exponent.

The results of our exponent analysis are summarized in Fig. 6 (circles and squares). For comparison, the exact J_z/J dependence of the exponents $\alpha_\mu, \beta_\mu, \mu = x, z$ is shown by four solid lines. With fewer than ten Δ_k's available, such an analysis is subject to considerable statistical and systematic uncertainty.

Starting at $J_z/J = 1$, our analysis correctly predicts an exponent $\alpha_x = \alpha_z$ near zero and an exponent $\beta_x = \beta_z$ very close to -1. For decreasing values of J_z/J, the increasing trend of α_z, β_z and the decreasing trend of α_x, β_x are both correctly reproduced by our estimates.

The results for the exponents α_x, α_z are evidently less accurate than those for β_x, β_z. The reason for this is the more complex structure of the autocorrelation functions $S^{\mu\mu}(\omega)$ as compared to the dynamic structure factors $S_{\mu\mu}(q,\omega)$. The former have a singularity at $\omega = \varepsilon_L(\pi/2)$ of 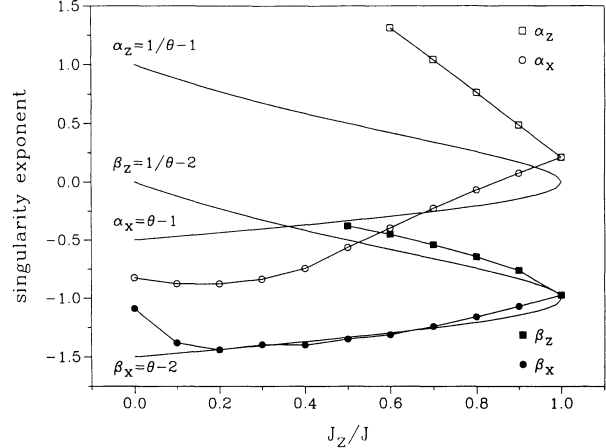strength comparable to that at $\omega = 0$. This second singularity is more likely to interfere with the simple pattern of the model $\bar{\Delta}_k$ sequence (2.18) on which our exponent estimates are based.

FIG. 6. Infrared-singularity exponents α_μ, β_μ, $\mu = x, z$ of $S^{\mu\mu}(\omega)$ and $S_{\mu\mu}(\pi,\omega)$ as functions of the anisotropy parameter J_z/J for the 1D $S = 1/2$ XXZ model at $T = 0$. The circles and squares represent the results derived as explained in the text from $K = 8$ nearly size-independent Δ_k's computed for a system of $N = 18$ spins. The exact results (3.6) are shown as solid lines.

More accurate exponent values can be obtained if more Δ_k's are available for the analysis. This expectation is supported by the following result: For $J_z/J = 0$ we can compute up to 13 completely size-independent Δ_k's from exactly known frequency moments.[6] When we use them all in our exponent analysis, we obtain a data point for α_x at $J_z = 0$ which is right on target.[22]

For the exponents α_z, β_z the analysis has only been carried out over a restricted parameter range $(0.5 \leq J_z/J \leq 1)$. In the weak-coupling regime, $J_z/J \ll 1$, of the corresponding lattice fermion system, an exponent analysis based on nearly size-independent Δ_k's is still possible but must proceed differently.[46]

IV. 2D $S = 1/2$ XXZ MODEL

Widespread interest in 2D quantum spin models was no doubt kindled by the excitement about the oxide high-T_c superconductors. The electronic properties of the CuO_2 planes in the undoped parent compound $La_2 CuO_4$ are describable, in some approximation, by the prototype model for a Mott insulator—the 2D Hubbard model. For very strong on-site repulsion, it turns into the 2D $S = 1/2$ Heisenberg antiferromagnet.[50,51] By embedding the latter in the more general XXZ model (1.1), we gain a parameter, J_z/J, which controls the direction of the magnetic ordering in the ground state. This enables us to identify and interpret finite-size effects even though our numerical analysis is limited to a single system size (4×4 lattice).

In a classical description, the $T = 0$ phase change at $J_z/J = 1$ consists of a simple spin-flop transition be-

tween two Néel states representing saturated antiferromagnetic long-range order parallel and perpendicular to the z axis. The two classical ground states are further distinguished by their degree of degeneracy. The one for $J_z/J > 1$, which breaks a discrete symmetry of H, is twofold degenerate, whereas the degeneracy of the other (for $J_z/J < 1$), which breaks a continuous symmetry of H, is proportional to the lattice size. Both types of degeneracy are removed in the presence of quantum fluctuations, and all finite-size ground-state properties change smoothly across the transition point $J_z/J = 1$. In finite systems, therefore, the characteristic signature of phase transitions must be searched in the dynamically relevant excitation spectrum. The most direct access to that spectrum is provided by the recursion method as we have already amply demonstrated for the 1D case.

A. Dynamic structure factors $S_{\mu\mu}(\pi, \pi, \omega)$

The numerical results presented here for the $T = 0$ dynamics of the 2D $S = 1/2$ XXZ model are all derived from the ground-state wave function of a 4×4 lattice with periodic boundary conditions. The question is then not how to avoid finite-size effects but how to identify them and how to estimate their impact. For the reconstruction of the functions $S_{\mu\mu}(\mathbf{q}, \omega)$, $\mu = x, z$ over the parameter range $0 \leq J_z/J \leq 2$, we have used the first six Δ_k's and a termination function selected according to the criteria spelled out in Appendix B. It is quite clear that not all six Δ_k's are nearly size independent.[26] We have indirect evidence that the number of nearly size-independent Δ_k's varies with J_z/J and is (not unexpectedly) lowest near the transition point. However, for our reconstruction procedure, we need at least five or six Δ_k's for the identification of the pattern, which determines the type of termination function to be used. Inevitably, they are strongly influenced by finite-size effects, at least in some instances. Nevertheless, observing the variation with J_z/J of the patterns in the Δ_k sequences yields important clues about changes in the structure of the ground state, specifically their nature and their location in parameter space.

Naturally, we wish to scrutinize the Δ_k sequences pertaining to $S_{\mu\mu}(\mathbf{q}, \omega)$, $\mu = x, z$ at the wave vector $\mathbf{q} = (\pi, \pi)$ associated with antiferromagnetic ordering. The one for $S_{zz}(\pi, \pi, \omega)$ shows a distinct type-2A pattern at small J_z/J, indicative of a spectral gap. With increasing J_z/J, that pattern is stable at first, then, at $J_z/J \simeq 0.9$ begins to change its character to a type-2B pattern, which reflects the emergence of a δ-function central peak as caused by antiferromagnetic long-range order in the z direction. That metamorphosis is completed at $J_z/J \simeq 1.3$. A similar change in pattern can be observed in the Δ_k sequence of $S_{xx}(\pi, \pi, \omega)$, but in opposite direction, i.e., from a type-2A pattern at $J_z/J > 1$ to a type-2B pattern at $J_z/J < 1$.[52] These changes of pattern together with the observation that no such changes occur in the Δ_k sequences for other wave vectors, clearly single out the phase diagram sketched in Fig. 1(b) from other possible scenarios. For comparison, recall that the

patterns in 1D were of type 2B for $S_{zz}(\pi, \omega)$ and of type 2A for $S_{xx}(\pi, \omega)$ at $J_z/J > 1$, where antiferromagnetic long-range order is established [see Fig. 1(a)], but of type 1 for both functions in the critical phase at $J_z/J \leq 1$.

The reconstructed functions $S^{\mu\mu}(\pi, \pi, \omega)$ themselves are displayed in Fig. 7 over a broad range of J_z/J values around the transition region. A general observation is that the spectral-weight distribution is considerably more localized than in $S_{\mu\mu}(\pi, \omega)$ of the 1D system. In the planar regime, $S_{xx}(\pi, \pi, \omega)$ is dominated by a narrow central peak, as is $S_{zz}(\pi, \pi, \omega)$ in the uniaxial regime.
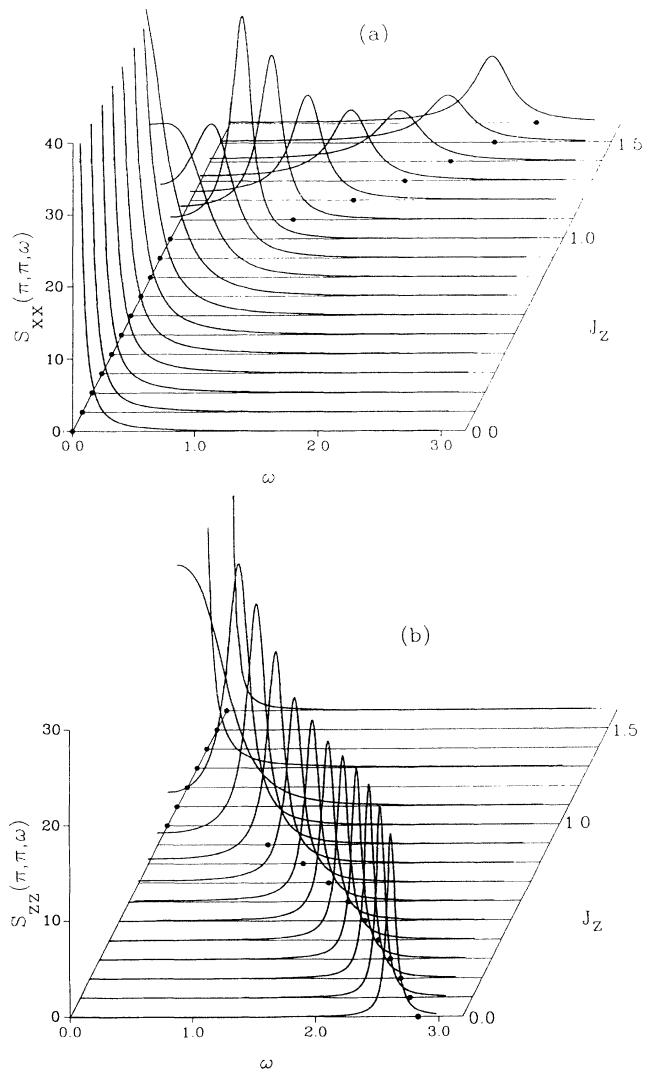

FIG. 7. Dynamic structure factors $S_{\mu\mu}(\mathbf{q}, \omega)$ at $T = 0$ for fixed $\mathbf{q} = (\pi, \pi)$ and (a) $\mu = x$, (b) $\mu = z$ of the 2D $S = 1/2$ XXZ model with $J = 1$ and $J_z = 0, 0.1, \ldots, 1.6$. The results are derived from the continued-fraction coefficients $\Delta_1, \ldots, \Delta_6$ and a matching termination function as described in the text. The circles in the (J_z, ω) plane mark the linear spin-wave frequency at $\mathbf{q} = (\pi, \pi)$ for that model in the Néel state, specifically the frequencies for modes involving spin fluctuations (a) perpendicular and (b) parallel to the z axis. For greater clarity, the curves at $J_z = 1.2, 1.4$, and 1.5 have been omitted in (b).

These central peaks, which originate from type-2B Δ_k sequences, represent the antiferromagnetic order parameter in the two phases, respectively. The nonzero width is entirely due to our use of the one-parameter terminator (B3) for the reconstruction procedure.[53]

The fluctuations transverse to the order parameter are reflected in $S_{xx}(\pi,\pi,\omega)$ at $J_z/J > 1$ and in $S_{zz}(\pi,\pi,\omega)$ at $J_z/J < 1$, in the form of well-defined peaks with nearly symmetric line shapes. The position of these peaks is in fair agreement with the prediction of linear spin-wave theory (to be discussed in Sec. IV C). However, let us keep in mind that linear spin waves are not exact eigenstates of the XXZ antiferromagnet and that the ground state is subject to correlated quantum fluctuations, which cause a partial reduction of the order parameter as discussed in the context of Fig. 1. All this will surely result in an intrinsic broadening of the spin-wave peak such as is evident in Fig. 7. Note that the spin-wave peaks as obtained from our reconstruction procedure do *not* represent individual poles of a truncated continued fraction [i.e., expression (2.5) with $b_K^2 = 0$] evaluated at $\zeta = \omega + i\varepsilon$ with $\varepsilon > 0$ to smear out the δ functions into Lorentzians.

B. Soft modes

On approach to the transition point $J_z/J = 1$ from either side, the spin-wave peaks at $\mathbf{q} = (\pi,\pi)$ become soft as expected, but the gap in the reconstructed functions $S_{\mu\mu}(\pi,\pi,\omega)$ reaches zero only somewhat beyond the transition point—a clear finite-size effect. Here, the coefficients $\Delta_1, \ldots, \Delta_6$ as extracted from the 4×4 system are more strongly size dependent than for other parameter values. In Fig. 8 we have plotted the peak posi-
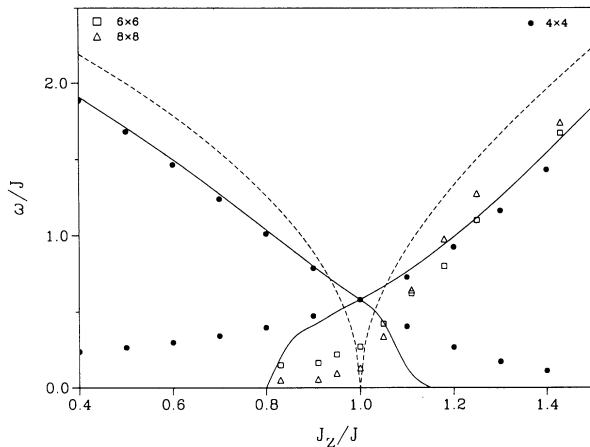

FIG. 8. Dependence on the anisotropy parameter J_z/J of the spectral gap between the ground state and the lowest transverse excitation at wave vector $\mathbf{q} = (\pi,\pi)$ for the 2D $S = 1/2\, XXZ$ model. The solid lines represent the spin-wave peak of the dynamic structure factors displayed in Fig. 7 (S_{zz} for $J_z/J \lesssim 1$ and S_{xx} for $J_z/J \gtrsim 1$). The full circles denote the exact spectral gaps of the 4×4 lattice. The open squares and triangles are spectral gaps for 6×6 and 8×8 lattices, respectively, as quoted from a quantum Monte Carlo study (Ref. 54). The linear spin-wave predictions are shown as dashed lines.

tions of the reconstructed $S_{\mu\mu}(\pi,\pi,\omega)$ as functions of J_z/J and the corresponding linear spin-wave frequencies. Also plotted are the exact spectral gaps between the ground state ($\mathbf{k} = \mathbf{0}$, $S_T^z = 0$) and the lowest state at $\mathbf{k} = (\pi,\pi)$ relevant for in-plane fluctuations ($S_T^z = \pm 1$) or out-of-plane fluctuations ($S_T^z = 0$), and corresponding quantum Monte Carlo data of Barnes et al.[54] for lattice sizes 6×6 and 8×8. In the transition region, the peak positions from Fig. 7 agree quite well with the spectral gaps of the 4×4 lattice, which confirms the strong size dependence of some of the coefficients $\Delta_1, \ldots, \Delta_K$ used for the reconstruction. However, unlike the 4×4 excitation gap, which stays nonzero throughout the parameter range shown in Fig. 8, the spin-wave peak of the reconstructed $S_{\mu\mu}(\pi,\pi,\omega)$ turns into a true central peak at the edge of the transition region. Here our input data $\Delta_1, \ldots, \Delta_K$ extracted from the 4×4 ground state are considerably less size dependent than the finite-size spectral gap. The linear spin-wave frequency of the transverse mode at the ordering wave vector goes to zero as $|J_z/J - 1|^{1/2}$ near the Heisenberg point in both 1D ($q = \pi$) and 2D [$\mathbf{q} = (\pi,\pi)$]. However, it is rigorously known in 1D that the lowest out-of-plane excitation at $q = \pi$ stays soft in the planar regime, and the lowest in-plane excitation rises by an exponential law in the uniaxial regime (see Fig. 1). It is not clear how accurate the spin-wave prediction near $J_z/J = 1$ is in the 2D case.[55]

The size dependence of the peak frequency in $S_{\mu\mu}(\mathbf{q},\omega)$ at $\mathbf{q} = (\pi,\pi)$ has been the object, directly or indirectly, of several studies based on a variety of methods. Our continued-fraction analysis for the 4×4 lattice ($N = 16$) yields $\omega/J \simeq 0.57$. Chen and Schüttler[56] carried out a different continued-fraction analysis and obtained peak frequencies of $\omega/J \simeq 2.0$, 1.0, and 0.58 for $N = 4$, 8, and 16, respectively. de Vries and de Raedt[57] solved the time-dependent Schrödinger equation numerically, employing the Lie-Trotter formula, and obtained peak frequencies $\omega/J \simeq 0.47$ and 0.39 for $N = 20$ and 26, respectively. Barnes et al.[54] calculated energy differences by the Lanczös method and the diffusion Monte Carlo method, and obtained $\omega/J \simeq 0.5786$, 0.27, and 0.13 for $N = 16$, 36, and 64, respectively. All these data are well in line with each other and with the predicted size dependence[58] $\omega/J = 8/N$.

C. Spin-wave dispersions

The well-defined spin-wave-like excitations observed[59] in La$_2$CuO$_4$ and also found in our analysis of the dynamic structure factors $S_{\mu\mu}(\pi,\pi,\omega)$ suggest that we extend the comparison of the continued-fraction analysis with spin-wave theory to the full Brillouin zone of the square lattice. As a starting point for the spin-wave analysis, we consider the d-dimensional hypercubic spin-S XYZ antiferromagnet with $J_z > J_x, J_y$. The dispersion of the linear spin waves, which are the normal modes transverse to the Néel state in the z direction (classical ground state) is then[60]

$$\omega_{\mathbf{k}}^2 = 4d^2 S^2 (J_z \pm J_x \gamma_{\mathbf{k}})(J_z \mp J_y \gamma_{\mathbf{k}}), \qquad (4.1)$$

where

$$\gamma_{\mathbf{k}} = \frac{1}{d} \sum_{\alpha=1}^{d} \cos k_{\alpha}. \qquad (4.2)$$

Applied to the 2D $S = 1/2$ XXZ model (1.1), this expression reduces to the branch

$$\omega_{\mathbf{k}} = 2J\sqrt{J_z^2/J^2 - \gamma_{\mathbf{k}}^2} \qquad (4.3)$$

for the uniaxial regime $(J_z > J_x = J_y \equiv J)$ and, after a rotation in spin space, to the two branches

$$\omega_{\mathbf{k}} = 2J\sqrt{(1 \pm \gamma_{\mathbf{k}})[1 \mp (J_z/J)\gamma_{\mathbf{k}}]} \qquad (4.4)$$

for the planar regime $(J_z < J)$. The two branches (4.4) correspond to in-plane (upper sign) and out-of-plane (lower sign) fluctuations, respectively.

The spin-wave dispersions (4.4) for the case $J_z/J = 0$ are plotted in Fig. 9(a) along a path through the Brillouin zone (see inset) which touches all $\mathbf{q}$ vectors of the 4×4 lattice. The circles and squares represent the peak positions of the reconstructed dynamic structure factors $S_{zz}(\mathbf{q}, \omega)$ and $S_{xx}(\mathbf{q}, \omega)$, respectively. The in-plane spin-wave mode (solid lines) becomes soft for $\mathbf{k} \to (\pi, \pi)$ $(\gamma_{\mathbf{k}} \to -1)$ with the staggered zero-frequency mode representing a rigid rotation of the order parameter in the xy plane. The out-of-plane fluctuations (dashed lines) on the other hand, have a soft mode at $\mathbf{k} = \mathbf{0}$ $(\gamma_{\mathbf{k}} = 1)$, but with zero intensity in $S_{zz}(\mathbf{0}, \omega)$ because of the conserved quantity $S_T^z = 0$. The overall agreement between the linear spin-wave prediction and the continued-fraction analysis is very satisfactory, indeed surprisingly good in view of the fact that the former is based on a caricature ground state and the latter on a miniature lattice.

The results of the two approaches deviate much more strongly for the model with isotropic exchange $(J_z/J = 1)$ as shown in Fig. 9(b). The linear spin-wave dispersions (4.4), now both identical with (4.3), are shown as solid lines and the peak positions of the reconstructed function $S_{xx}(\pi, \pi, \omega) = S_{zz}(\pi, \pi, \omega)$ for the 4×4 lattice as circles. There is now a significant mismatch in the overall frequency scale, and the (π, π) mode of the continued-fraction analysis is not really soft for reasons explained in Sec. IV A.

For comparison we have included in Fig. 9(b) the dispersion, proportional to $\sqrt{\sin^2 k_x + \sin^2 k_y}$ (short-dashed lines), inferred by Wang[61] from an approximate calculation based on a 2D application of the Jordan-Wigner transformation between spins with $S = 1/2$ and lattice fermions.[62] It differs from the spin-wave dispersion most strongly along the $(1, 0)$ direction. Our data point at $\mathbf{q} = (\pi, 0)$ seems to rule out Wang's dispersion, but the catch is that the nearest-neighbor periodic 4×4 square is topologically equivalent to a 4D nearest-neighbor periodic $2 \times 2 \times 2 \times 2$ hypercube,[63] implying equivalence

of $\mathbf{q} = (\pi, 0)$ and $\mathbf{q} = (\pi/2, \pi/2)$. For completely unrelated reasons, the spin-wave dispersion too yields the same frequency at those two wave vectors.

The intrinsically classical linear spin-wave dispersion derived above is renormalized by quantum and nonlinear effects, which may be taken into account in higher-order spin-wave theory. As shown in a recent study[64] of the Heisenberg $(J_z/J = 1)$ model, this leads to a weak three-magnon continuum in the dynamic structure factor, in addition to the single-magnon (δ-function) peak. The position of that peak marks the renormalized spin-wave frequency, which differs from (4.3) by a factor in the range between 1.2 and 1.4 over most of the Brillouin zone, in agreement with a series expansion (in J/J_z)[65] combined with the single-mode approximation[66]. That would bring the spin-wave curves in Fig. 9(b) much closer to the data points at $\mathbf{q} \neq (\pi, \pi)$ of our continued-fraction analysis.[67]
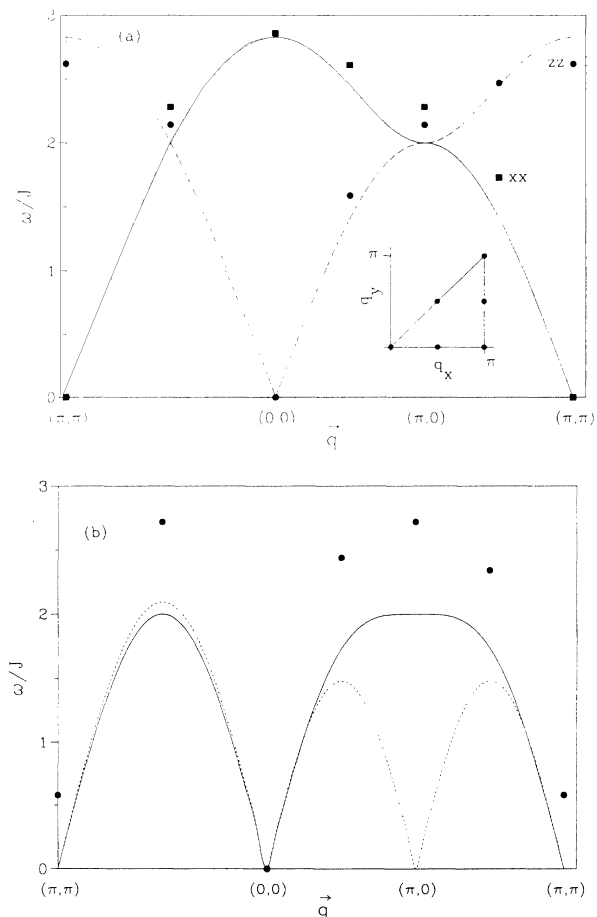

FIG. 9. Spin-wave dispersion relations for the 2D $S = 1/2$ XXZ model with (a) $J_z/J = 0$, (b) $J_z/J = 1$. The solid and dashed lines in (a) represent the in-plane and out-of-plane linear spin-wave modes, respectively, as given in Eq. (4.4). In (b) the two linear spin-wave modes (4.4) coalesce and are plotted as solid line. The short-dashed line in (b) is Wang's result derived in the fermion representation. The peak positions of the dynamic structure factors $S_{xx}(\mathbf{q}, \omega)$ and $S_{zz}(\mathbf{q}, \omega)$ obtained by the recursion method for the 4×4 lattice are shown as full squares and circles, respectively.

ACKNOWLEDGMENTS

APPENDIX A: FREQUENCY MOMENTS AND CONTINUED-FRACTION COEFFICIENTS

In the power series of the normalized correlation function,

$$D_0(t) = \frac{\langle A^\dagger(t)A \rangle}{\langle A^\dagger A \rangle} = \sum_{n=0}^{\infty} M_n \frac{(-it)^n}{n!}, \tag{A1}$$

the coefficients M_{2k} of the real, symmetric part are the same as those in the expansion of the normalized fluctuation function

$$C_0(t) = \frac{(A(t), A)}{(A, A)} = \sum_{k=0}^{\infty} \frac{(-1)^k}{2k!} M_{2k} t^{2k}. \tag{A2}$$

The M_{2k} are the even frequency moments of both the (normalized) structure function $S_0(\omega) \equiv S(\omega)/\langle A^\dagger A \rangle$ and the spectral density $\Phi_0(\omega)$. The odd moments M_{2k+1} of $S_0(\omega)$ can be derived, via the Kramers-Kronig relations, from the even moments M_{2k} provided the full set is known. In the present study we only use a finite number of M_{2k}'s (converted into an equal number of Δ_k's). The Hamiltonian representation of the recursion method produces pairs of continued-fraction coefficients a_k, b_k^2 for the function $d_0(\zeta)$. They can be converted into an equal number of moments M_n for the function $D_0(t)$ and vice versa by a simple algorithm as follows. By Laplace transform (2.4) the power series (A1) becomes an asymptotic expansion

$$d_0(\zeta) = i \sum_{n=0}^{\infty} M_n \zeta^{-(n+1)}, \tag{A3}$$

which, when compared to the same function in the continued-fraction representation (2.5), yields a set of relations between the continued-fraction coefficients a_k, b_k^2 and the moments M_n. Those relations are most easily expressed in terms of two arrays of auxiliary quantities $L_k^{(n)}$ and $M_k^{(n)}$.

Given a set of moments $M_0 \equiv 1, M_1, \ldots, M_{2K+1}$, the continued-fraction coefficients $a_0, \ldots, a_K$ and $b_1^2, \ldots, b_K^2$ are obtained by initializing

$$M_k^{(0)} = (-1)^k M_k \ , \ L_k^{(0)} = (-1)^{k+1} M_{k+1}, \tag{A4}$$

for $k = 0, \ldots, 2K$ and then applying the recurrence relations

$$M_k^{(n)} = L_k^{(n-1)} - L_{n-1}^{(n-1)} \frac{M_k^{(n-1)}}{M_{n-1}^{(n-1)}}, \tag{A5a}$$

$$L_k^{(n)} = \frac{M_{k+1}^{(n)}}{M_n^{(n)}} - \frac{M_k^{(n-1)}}{M_{n-1}^{(n-1)}}, \tag{A5b}$$

for $k = n, \ldots, 2K - n + 1$ (in two successive inner loops) and $n = 1, \ldots, 2K$ (outer loop). The resulting continued-fraction coefficients are

$$b_n^2 = M_n^{(n)} \ , \ a_n = -L_n^{(n)} \ , \ n = 0, \ldots, K. \tag{A6}$$

In the reverse direction, the proper initialization is

$$M_n^{(n)} = b_n^2 \ , \ L_n^{(n)} = -a_n \ , \ n = 0, \ldots, K, \tag{A7}$$

(where $b_0^2 \equiv 1$, $b_{-1}^2 \equiv 1$), and

$$M_k^{(-1)} = 0 \ , \ k = 0, \ldots, 2K + 1. \tag{A8}$$

The recurrence relations to be carried out for $n = 0, \ldots, \min(K, 2K - j)$ (inner loop) and $j = 0, \ldots, 2K + 1$ (outer loop) are

$$M_{n+j+1}^{(n)} = b_n^2 L_{n+j}^{(n)} + \frac{b_n^2}{b_{n-1}^2} M_{n+j}^{(n-1)}, \tag{A9a}$$

$$L_{n+j+1}^{(n)} = M_{n+j+1}^{(n+1)} - \frac{a_n}{b_n^2} M_{n+j+1}^{(n)}, \tag{A9b}$$

The moments are then given by

$$M_n = (-1)^n M_n^{(0)} \ , \ n = 0, \ldots, 2K + 1. \tag{A10}$$

The even moments $M_0, \ldots, M_{2K}$ resulting from that procedure may then be used to construct the Δ_k's ($k = 1, \ldots, K$) by a similar recursive scheme:[68] Initialize

$$M_{2k}^{(0)} = M_{2k}, \ M_{2k}^{(-1)} = 0, \ k = 0, \ldots, K \tag{A11}$$

and $\Delta_{-1} = \Delta_0 = 1$, then execute (for $m = 1, 2, \ldots, K$)

$$M_{2k}^{(m)} = \frac{M_{2k}^{(m-1)}}{\Delta_{m-1}} - \frac{M_{2k-2}^{(m-2)}}{\Delta_{m-2}}, \ k = m, m+1, \ldots, K \tag{A12}$$

and collect the desired coefficients

$$\Delta_m = M_{2m}^{(m)}. \tag{A13}$$

APPENDIX B: RECONSTRUCTION PROCEDURE

Consider the model spectral density (2.19) with $A = 0$, which is a Gaussian of width ω_0 split at the center to produce a gap of size 2Ω. The associated model $\bar{\Delta}_k$ sequence can be generated numerically, as explained in Appendix A, from the exact frequency moments,

$$\bar{M}_{2k} = 2\pi \sum_{m=0}^{k} \binom{2k}{2m} \frac{\omega_0^{2m} \Omega^{2(k-m)}}{2^m} (2m - 1)!!$$

$$+ 2\sqrt{\pi} \sum_{m=0}^{k-1} \binom{2k}{2m+1} \Omega^{2(k-m)-1} \omega_0^{2m+1} m! \tag{B1}$$

with $(-1)!! \equiv 1$. As a first step in the reconstruction of the relaxation function $\tilde{c}_0(z)$ from a type-2A sequence $\Delta_1, \ldots, \Delta_K$ (the data produced by some application of the recursion method) we determine the parameters Ω and ω_0 of the model spectral density $\bar{\Phi}_0(\omega)$ by minimizing the quantity

$$\sum_{k=1}^{K} \frac{1}{k} |\Delta_k - \bar{\Delta}_k|. \tag{B2}$$

This particular criterion turned out to be the most reliable and robust one in a series of tests.

In the second step, the model relaxation function $\bar{c}_0(z)$ is determined by a numerical evaluation of the Hilbert transform (2.21) and then expanded into a continued fraction with the known model coefficients $\bar{\Delta}_k$ down to level K as in (2.20). This determines the model termination function $\bar{\Gamma}_K(z)$. Replacing the model coefficients $\bar{\Delta}_1, \ldots, \bar{\Delta}_K$ in the expansion of $\bar{c}_0(z)$ by the system coefficients $\Delta_1, \ldots, \Delta_K$ yields the reconstructed relaxation function $\tilde{c}_0(z)$, which, evaluated near the physical frequency axis (we use $z = \varepsilon - i\omega$, $\varepsilon = 10^{-3} J$) becomes the reconstructed spectral density.

The worst that can happen if this procedure is applied to a type-2A Δ_k sequence is that the fit (B2) overestimates the spectral gap in the sense that it produces a value for the gap parameter Ω that is not completely consistent with the known coefficients $\Delta_1, \ldots, \Delta_K$. In that (rare) event, the reconstructed spectral density ex-

hibits an artifact that is easy to recognize, namely a dip at $\omega = \Omega$ and a spectral spike at some lower frequency. This artifact can be removed by choosing a lower value for the gap parameter. Much less harm is done if the fit (B2) underestimates the true spectral gap. The spectral weight is then not strictly zero where it should be; instead it tapers off continuously albeit rapidly, if the mismatch is not too large.

For the present study, we have used the model spectral density (2.19) with $A = 0$ also for type-2B and type-1 Δ_k sequences. Here the gap parameter Ω turns out to be zero and (2.19) reduces to a one-parameter Gaussian:

$$\bar{\Phi}_0(\omega) = \frac{2\sqrt{\pi}}{\omega_0} e^{-\omega^2/\omega_0^2} \quad , \quad \bar{\Delta}_k = \frac{1}{2}\omega_0^2 k. \tag{B3}$$

This choice has the advantage that it is completely unbiased with respect to any structural detail in the reconstructed spectral density. Artificial structures are then unlikely to make their appearance. The price to be paid is that some genuine structural features are less focused than they could be: Type-1A spectral densities reconstructed with (2.17) would have real infrared divergences, whereas reconstruction with (B3) results in central peaks of finite height. Likewise, type-2B spectral densities reconstructed with (2.19) would have a real spectral line at the center of the gap as opposed to a central peak of finite height and width, albeit very tall and narrow if the reconstruction is carried out with (B3).

---

* On leave from Institut für Physik, Universität Dortmund, 44221 Dortmund, Germany.

[1] R. Orbach, Phys. Rev. **112**, 309 (1958); J. Des Cloizeaux and M. Gaudin, J. Math. Phys. **7**, 1384 (1966); C. N. Yang and C. P. Yang, Phys. Rev. **150**, 321 (1966).

[2] R. J. Baxter, J. Stat. Phys. **9**, 145 (1973).

[3] A. Luther and I. Peschel, Phys. Rev. B **12**, 3908 (1975); F. D. M. Haldane, Phys. Rev. Lett. **45**, 1358 (1980); J. L. Black and V. J. Emery, Phys. Rev. B **23**, 429 (1981); M. P. M. Den Nijs, ibid. **23**, 6111 (1981).

[4] B. M. McCoy, E. Barouch, and D. B. Abraham, Phys. Rev. A **4**, 2331 (1971); B. M. McCoy, J. H. H. Perk, and R. E. Shrock, Nucl. Phys. B **220** [FS8], 35 (1983).

[5] T. Niemeijer, Physica **36**, 377 (1967); S. Katsura, T. Horiguchi, and M. Suzuki, ibid. **46**, 67 (1970).

[6] G. Müller and R. E. Shrock, Phys. Rev. B **29**, 288 (1984).

[7] K. Kubo and T. Kishi, Phys. Rev. Lett. **61**, 2585 (1988).

[8] K. Kubo, Phys. Rev. Lett. **61**, 110 (1988).

[9] Y.Ozeki, H. Nishimori, and Y. Tomita, J. Phys. Soc. Jpn. **58**, 82 (1989).

[10] H. A. Wischmann and E. Müller-Hartmann, J. Phys. I (France), **1**, 647 (1991).

[11] J. D. Reger and A. P. Young, Phys. Rev. B **37**, 5978 (1988).

[12] M. Gross, E. Sanchez-Velasco, and E. Siggia, Phys. Rev. B **39**, 2484 (1989).

[13] H.-Q. Ding and M. S. Makivic, Phys. Rev. Lett. **64**, 1449 (1990); M. S. Makivic and H.-Q. Ding, Phys. Rev. B **43**, 3562 (1991).

[14] K. J. Runge, Phys. Rev. B **45**, 7229 (1992).

[15] M. Kikuchi and Y. Okabe, J. Phys. Soc. Jpn. **58**, 679

(1989).

[16] T. Barnes, D. Kotchan, and E. S. Swanson, Phys. Rev. B **39**, 4357 (1989).

[17] N. D. Mermin and H. Wagner, Phys. Rev. Lett. **17**, 1133 (1966).

[18] R. Haydock, Solid State Phys. **35**, 215 (1980).

[19] The recursion method and its applications, edited by D. G. Pettifor and D. L. Weaire (Springer-Verlag, New York, 1985).

[20] M. H. Lee, Phys. Rev. B **26**, 2547 (1982).

[21] E. R. Gagliano, E. Dagotto, A. Moreo, and F. C. Alcaraz, Phys. Rev. B **34**, 1677 (1986).

[22] V. S. Viswanath and G. Müller, J. Appl. Phys. **67**, 5486 (1990).

[23] H. Nishimori and Y. Taguchi, Prog. Theor. Phys. Suppl. **87**, 247 (1986).

[24] W. W. Bradbury and R. Fletcher, Num. Math. **9**, 259 (1966).

[25] M. P. Nightingale, V. S. Viswanath, and G. Müller, Phys. Rev. B **48**, 7696 (1993).

[26] Finite-size effects in the Δ_k sequence have basically two origins: (i) The finite-size ground-state wave function causes, in general, a *weak* size dependence of the Δ_k's. (ii) Each Δ_k is expressible in terms of equal-time correlation functions involving spin operators for clusters of sites on the finite lattice. For autocorrelation functions of a Hamiltonian with nearest-neighbor interaction, as an example, the linear dimension of the largest clusters is $2k + 1$. Consequently, the Δ_k's start to become *strongly* size-dependent when $2k + 1 > N^{1/d}$, i.e., when the clusters start to wrap

around the finite lattice.

[27] A. Magnus, in *The Recursion Method and its Applications* (Ref. 19), p. 22; D. S. Lubinsky, Acta Applic. Math. **10**, 237 (1987).

[28] J.-M. Liu and G. Müller, Phys. Rev. A **42**, 5854 (1990).

[29] V. S. Viswanath and G. Müller, J. Appl. Phys. **70**, 6178 (1991).

[30] If two normalized spectral densities $\Phi(\omega)$ and $\tilde{\Phi}(\omega)$ differ only by a peak $\propto \delta(\omega)$, the two Δ_k sequences are related by $\Delta_{2n} + \Delta_{2n-1} = \tilde{\Delta}_{2n} + \tilde{\Delta}_{2n-1}$.

[31] Even when the finite-size ground state does not exhibit true long-range order, the nearly size-independent Δ_k's bear its characteristic signature.

[32] G. Müller, H. Thomas, M. W. Puga, and H. Beck, J. Phys. C **14**, 3399 (1981).

[33] The model spectral density (B3) is also used for the reconstruction of $S_{xx}(0,\omega)$ except for $J_z/J = 1$, where the intensity is zero.

[34] It is instructive to compare our result for $S_{xx}(\pi,\omega)$ shown in Fig. 4(a), which is inferred from six nearly size-independent Δ_k's of a system of size $N = 16$ with the same function plotted in Fig. 4 of S. Haas, J. Riera, and E. Dagotto, Phys. Rev. B, **48**, 3281 (1993), which was reconstructed from a large number of continued-fraction coefficients with strong size dependence except for the first few and for a much larger system ($N = 26$).

[35] J. Deisz, M. Jarrell, and D. L. Cox, Phys. Rev. B **42**, 4869 (1990).

[36] The artifacts produced by our numerical analysis when it underestimates or overestimates the spectral gap are described in Appendix B.

[37] G. Müller, H. Thomas, H. Beck, and J. C. Bonner, Phys. Rev. B **24**, 1429 (1981).

[38] T. Schneider, E. Stoll, and U. Glaus, Phys. Rev. B **26**, 1321 (1982).

[39] P. C. Hohenberg and W. F. Brinkman, Phys. Rev. B **10**, 128 (1974).

[40] G. Müller, Phys. Rev. B **26**, 1311 (1982).

[41] T. Todani and K. Kawasaki, Prog. Theor. Phys. **50**, 1216 (1973).

[42] H. Beck and G. Müller, Solid State Commun. **43**, 399 (1982).

[43] H. C. Fogedby, J. Phys. C **11**, 4767 (1978).

[44] A. Luther and I. Peschel (Ref. 3).

[45] S. E. Nagler, D. A. Tennant, R. A. Cowley, T. G. Perring, and S. K. Satija, Phys. Rev. B **44**, 12 361 (1991).

[46] The results of that analysis will be reported elsewhere [V. S. Viswanath, J. Stolze, and G. Müller (unpublished)].

[47] The exact result for $J_z/J = 0$ has a logarithmic divergence at $\omega/J = 1$.

[48] H. J. Schulz and T. Ziman, Phys. Rev. B **33**, 6545 (1986).

[49] Here we use $K = 8$ nearly size-independent Δ_k's extracted from the $N = 18$ ground state.

[50] E. Manousakis, Rev. Mod. Phys. **63**, 1 (1991).

[51] T. Barnes, Int. J. Mod. Phys. B **2**, 659 (1991).

[52] In practice, the Δ_k sequences of $S_{xx}(\pi,\pi,\omega)$ and $S_{zz}(\pi,\pi,\omega)$ at $J_z/J = 1$ are not identical due to numerical inaccuracies. We use these differences to assess the overall accuracy of the calculation. In our experience, a high numerical precision is required for all steps of the calculation, including the determination of the ground-state wave function.

[53] When we use instead the three-parameter terminator (2.19), the central peak becomes a true δ function, but fitting six data points with three parameters introduces potential biases whose adverse effects outweigh the benefit of having a δ-function central peak.

[54] T. Barnes, K. J. Cappon, E. Dagotto, D. Kotchan, and E. S. Swanson, Phys. Rev. B **40**, 8945 (1989).

[55] See C. J. Hamer, W. Zheng, and P. Arndt, Phys. Rev. B **46**, 6276 (1992) for a discussion of higher-order spin-wave and series-expansion results for the gap in the uniaxial regime.

[56] C.-X. Chen and H.-B. Schüttler, Phys. Rev. B **40**, 239 (1989).

[57] P. de Vries and H. de Raedt, Phys. Rev. B **47**, 7929 (1993).

[58] W. Zheng and C. J. Hamer, Phys. Rev. B **47**, 7961 (1993).

[59] S. M. Hayden, G. Aeppli, R. Osborn, A. D. Taylor, T. G. Perring, S.-W. Cheong, and Z. Fisk, Phys. Rev. Lett. **67**, 3622 (1991).

[60] D. C. Mattis, *Theory of Magnetism*, 2nd ed. (Springer-Verlag, New York, 1981); J. Kurmann, H. Thomas, and G. Müller, Physica A **112**, 235 (1982).

[61] Y. R. Wang, Phys. Rev. B **46**, 151 (1992).

[62] The lattice fermions interact via short-range (density-density) as well as long-range (gauge) interactions. Wang's mean-field treatment decouples the short-range interaction and replaces the long-range interaction by an effective vector potential distributed over the lattice in a certain pattern.

[63] K. Fabricius, U. Löw, and K.-H. Mütter, Phys. Rev. B **44**, 9981 (1991).

[64] C. M. Canali and M. Wallin, Phys. Rev. B **48**, 3264 (1993).

[65] R. R. P. Singh, Phys. Rev. B **47**, 12 337 (1993).

[66] The single-mode approximation [R. P. Feynman, Phys. Rev. **94**, 262 (1954)] provides an upper bound to the frequency of the lowest dynamically relevant excitation by the (normalized) first moment a_0 of the unsymmetrized $T = 0$ structure function (2.6) (which vanishes for $\omega < 0$). Technically, the single-mode approximation means $b_1^2 \equiv 0$ in (2.5). A similar approximation, $\Delta_2 \equiv 0$ in (2.13), approximates the spectrum by a single line at $\omega = \Delta_1^{1/2} = (a_0^2 + b_1^2)^{1/2}$. The difference between the squares of those two frequencies thus estimates the width of the spectral density, $b_1^2 = \langle \omega^2 \rangle - \langle \omega \rangle^2$.

[67] For $J_z/J > 1$ the dispersion of the $S_{xx}(\mathbf{q},\omega)$ peak frequency becomes increasingly flat throughout the Brillouin zone and is (not surprisingly) very well described by linear spin-wave theory. The peak frequency of $S_{zz}(\mathbf{q},\omega)$ in the uniaxial regime is higher than that of $S_{xx}(\mathbf{q},\omega)$ and does not vary too much throughout the Brillouin zone except for zeros at $\mathbf{q} = 0$ (due to the conservation of S_T^z) and $\mathbf{q} = (\pi,\pi)$ (due to antiferromagnetic order).

[68] M. Böhm, V. S. Viswanath, J. Stolze, and G. Müller (unpublished).